IEEE Journal of Translational Engineering in Health and Medicine

Received 28 February 2024; revised 11 June 2024; accepted 5 July 2024.
Date of publication 8 July 2024; date of current version 22 July 2024.

*Digital Object Identifier 10.1109/JTEHM.2024.3425269*

# Equivalent Electrical Circuit Approach to Enhance a Transducer for Insulin Bioavailability Assessment

**FRANCESCA MANCINO[1], (Student Member, IEEE), HANEN NOURI[2], NICOLA MOCCALDI[1], (Senior Member, IEEE), PASQUALE ARPAIA[1], (Senior Member, IEEE), AND OLFA KANOUN[2], (Senior Member, IEEE)**

[1]Department of Electrical Engineering and Information Technology (DIETI), University of Naples Federico II, 80125 Naples, Italy
[2]Department of Electrical Engineering and Information Technology, Chemnitz University of Technology, 09107 Chemnitz, Germany

CORRESPONDING AUTHOR: P. ARPAIA (pasquale.arpaia@unina.it)

**ABSTRACT** The equivalent electrical circuit approach is explored to improve a bioimpedance-based transducer for measuring the bioavailability of synthetic insulin already presented in previous studies. In particular, the electrical parameter most sensitive to the variation of insulin amount injected was identified. Eggplants were used to emulate human electrical behavior under a quasi-static assumption guaranteed by a very low measurement time compared to the estimated insulin absorption time. Measurements were conducted with the EVAL-AD5940BIOZ by applying a sinusoidal voltage signal with an amplitude of 100 mV and acquiring impedance spectra in the range [1–100] kHz. 14 units of insulin were gradually administered using a Lilly's Insulin Pen having a 0.4 cm long needle. Modified Hayden's model was adopted as a reference circuit and the electrical component modeling the extracellular fluids was found to be the most insulin-sensitive parameter. The trnasducer achieves a state-of-the-art sensitivity of 225.90 $ml^{-1}$. An improvement of 223 % in sensitivity, 44 % in deterministic error, 7 % in nonlinearity, and 42 % in reproducibility was achieved compared to previous experimental studies. The clinical impact of the transducer was evaluated by projecting its impact on a Smart Insulin Pen for real-time measurement of insulin bioavailability. The wide gain in sensitivity of the bioimpedance-based transducer results in a significant reduction of the uncertainty of the Smart Insulin Pen. Considering the same improvement in in-vivo applications, the uncertainty of the Smart Insulin Pen is decreased from 4.2 $\mu$l to 1.3 $\mu$l.
Clinical and Translational Impact Statement: A Smart Insulin Pen based on impedance spectroscopy and equivalent electrical circuit approach could be an effective solution for the non-invasive and real-time measurement of synthetic insulin uptake after subcutaneous administration.

**INDEX TERMS** Bioimpedance spectroscopy, equivalent circuit approach, insulin bioavailability, diabetes, metrological characterization, smart transducer.

## I. INTRODUCTION

TODAY, 10 million people are affected by type 1-diabetes [1]. This resulted from autoimmune damage of insulin-delivering $\beta$ cells of the pancreas by the defense system [2], [3]. Therefore, the patients need lifelong control of the impact of exogenous insulin administrations on levels of glucose in their blood [4], [5]. In the last years, technological developments have enabled non-invasive monitoring of blood glucose levels. However, the sensors exhibit poor sensitivity (i.e., resonator-based biosensors [6], [7], [8]), are still too expensive (i.e., 3-D printed sensors [9]), or are not adequately accurate for healthcare application (i.e., infrared spectroscopy-based sensors [10], [11], [12]).

To date, the Artificial Pancreas (AP) is the most widely used semi-automatic treatment to regulate glucose levels [13]. However, even equipped with the most recent glucose sensors, AP does not manage the unpredictable changes in glucose levels due to food ingestion. For this reason, the patient administers insulin manually before meals. The bolus is calculated by external systems requiring several

control inputs (e.g., insulin sensitivity factor, ISF, and insulin duration of action, IDA) depending on insulin uptake kinetics (bioavailability). Nowadays, ISF and IDA are defined only once by the diabetologists at the beginning of treatments, even if they are affected by different skin conditions/alterations (e.g., lipodystrophy) [14]. Currently, the insulin bioavailability has been extensively studied only when the drug has already been introduced into the bloodstream [15], [16], [17]. However, there are no in-vivo or non-invasive studies on measurement of the insulin bioavailability administered subcutaneously [13], [18], [19], [20]. Nowadays, indirect method for assessment of insulin bioavailability exhibits huge delays and are invasive (e.g., suction blister [21], and skin biopsies [22]) or are not reproducible (e.g., tape stripping [23], and micro dialysis [24]) or can only investigate the most superficial skin layers and are very costly (e.g., confocal Raman spectroscopy [25]). Also glucose sensors exhibit huge delays even if they are low-cost and non-invasive. To date, the impedance-based method results an approach to provide non-invasive, low-cost, and real-time measurements simultaneously. This method is extensively used in several biomedical applications [26], [27], [28], [29], [30], [31]. In [32] and [33], a bioimpedance analysis (BIA)-based transducer was prototyped and validated to assess the quantity of a substance (i.e., vehicle and insulin) still in situ after injections. In particular, the transducer identifies a personalized linear model (appearance model) relating the impedance magnitude to the quantity of substance delivered. To handle the inter- and intra-variability of the patients, the measurement method implements a real-time self-calibration. A new appearance model (namely, a new calibration diagram) linking amounts of injected insulin with the impedance magnitude is identified. In clinical applications, the transducer is supposed to be integrated into a Smart Insulin Pen for real-time measurements of insulin bioavailability. In particular, by inverting the calibration diagram of the transducer, the measurement model (disappearance model) of the Smart Insulin Pen is obtained. The disappearance model (obtained by inverting the appearance model) can be used to predict the amount of insulin gradually leaving the tissue under test and entering the circulatory system. Preliminary tests exhibited an uncertainty of 4.2 $\mu$l in measuring insulin absorption. [32]. Typically, insulin bolus disappears from the injection site in about 3 hours. [34], namely around 1 $\mu$l/min according to a linear approximation of the absorption trend. Lower uncertainty would reduce the time needed to appreciate the beginning of insulin absorption after injections, thus improving performance in clinical applications.

In the present paper, bioimpedance spectroscopy (BIS) measurement method and equivalent circuit approach were explored to achieve a state-of-the-art non-invasive measurement of insulin bioavailability. In comparison to BIA generally used to describe single-frequency impedance measurements, BIS is generally referred to frequency sweep impedance measurements [35], [36]. Therefore, the BIS method was exploited for improving the sensitivity of the proposed method and consequently achieving a measurement uncertainty compatible with clinical standards.

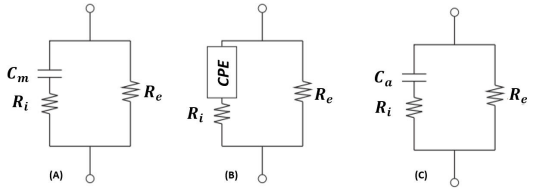


**FIGURE 1. Equivalent circuits for biological tissues: (A) Hayden's model, (B) Modified Hayden's model, and (C) Apparent capacitance-based model.**

The basis of electrical equivalent modeling specifically for biological tissue are presented in Section II; the bioimpedance transducer architecture is described in Section III. Finally, the experimental results on eggplants are reported in Section IV.

## II. BACKGROUND

In the conductometric field, a biological tissue can be approximately modeled as an electrolyte solution composed of a large number of cells [37], [38]. Conductivity measurements can be used to determine the quantity of solute in a solution. Similarly, impedance measurements can be used to determine the amount of drug injected into a biological tissue characterized by electrical conductivity and dielectric permittivity [39].

The electrical equivalent circuit approach proved to be suitable for modeling the electrical properties of different biologic tissues. Biological tissues are characterized by clusters of cells. A cell is composed of intracellular fluid (salts, proteins, and water) exhibiting a typical resistive behaviour and enveloped by the cell membrane (developed with protein-lipid-protein sandwich structure) exhibiting a typical capacitive behaviour [40], [41]. The cell is suspended in extracellular fluids (collection of molecules secreted by cells) [42], [43] with resistive behaviour [44]. The intracellular and extracellular fluids are conductive because of the dissolved ions, while the cell membrane acts as a dielectric [45], similarly to a capacitor where intracellular and extracellular fluid are the armature [46]. In the context of vegetable analysis, an effort has been made by Hayden to find an electrical equivalent model for describing the electrical behavior of vegetables [40], [47], [48].The Hayden model (Fig. 1.A) consists of a resistor in parallel with a series combination of a resistor and a capacitor. The intracellular and extracellular fluids are represented by resistances, while the cell membrane is described by capacitance. The modified Hayden model (Fig. 1.B) was introduced to better adapt the model to the vegetable tissue properties by replacing the capacitor with a constant phase element [49]. In this way, it was possible to take into account the dielectric dispersivity of vegetables.

In particular, the constant-phase distributed response element (CPE) is introduced to model a frequency-dependent

IEEE Journal of Translational Engineering in Health and Medicine

capacitance:

$$Z_{CPE} = \frac{1}{(j\omega)^p T} = \frac{cos(\frac{\pi}{2}p)}{\omega^p T} - j\frac{sin(\frac{\pi}{2}p)}{\omega^p T} \quad (1)$$

where:

- j is the imaginary unit;
- $\omega$ the angular frequency;
- T a constant;
- p an exponent in the range [0,1] representing the time constant distribution of the system.

The impedance of the Modified Hayden's Model ($Z_{MM}$) is:

$$Z_{MM} = R_{MM} - jX_{MM} \quad (2)$$

$$R_{MM} = \frac{R_e[1 + \omega^p T(2R_i + R_e)cos(\frac{\pi}{2}p) + \omega^p T R_i(R_e + R_i)}{\omega^p T(R_e + R_i)^2 + 2\omega^p T(R_e + R_i)cos(\frac{\pi}{2}p) + 1} \quad (3)$$

$$X_{MM} = \frac{\omega^p T R_e^2 sin(\frac{\pi}{2}p)}{\omega^p T(R_e + R_i)^2 + 2\omega^p T(R_e + R_i)cos(\frac{\pi}{2}p) + 1} \quad (4)$$

where $R_e$ and $R_i$ represent the extracellular and the intracellular equivalent resistance, respectively. A third model (Fig. 1.C) is adopted for describing the effect of the cell membrane capacitance [49], [50], [51], by introducing a new parameter:

$$C_a = T^{\frac{1}{p}}(R_e + R_i)^{(\frac{1-p}{p})} \quad (5)$$

To date, these models were used to describe several biological phenomena (e.g., solution absorption [52], ripening [53], drying/freezing treatments [49], [54], and hydration/dehydration process [49], [55], [56]). In [52], the impact of saline solution absorption on olive shoots was investigated. In particular, an evident reduction of extracellular resistance by increasing the saline concentration was experienced. In [53], the impedance variation of bananas due to ripening (reduction of ion, acid, and salt parts) was analyzed. Results showed an increment in the real impedance component and a decrease in the imaginary component. As far as the drying treatment is concerned, [49] and [54] highlighted an increment in impedance magnitude according to the drying proceeds. Finally, a decrease in extracellular resistance due to the hydration process was shown in [49], [56].

## III. ARCHITECTURE

The Smart Insulin Pen is a portable device able to measure the amount of insulin gradually absorbed (namely, bioavailability) through impedance measurements of the injection site. The Smart Insulin Pen is composed of a Bioimpedance Transducer calibrated at each new insulin administration. During the calibration phase, the parameters of a linear model (calibration diagram) linking the amount of insulin injected (input) and the impedance variation (output) are identified. By inverting the calibration diagram of Bioimpedance Transducer, the measurement model of the Smart Insulin Pen is obtained and it is used to compute the amount of drug migrated from the site of injection into the capillary (namely, bioavailability).

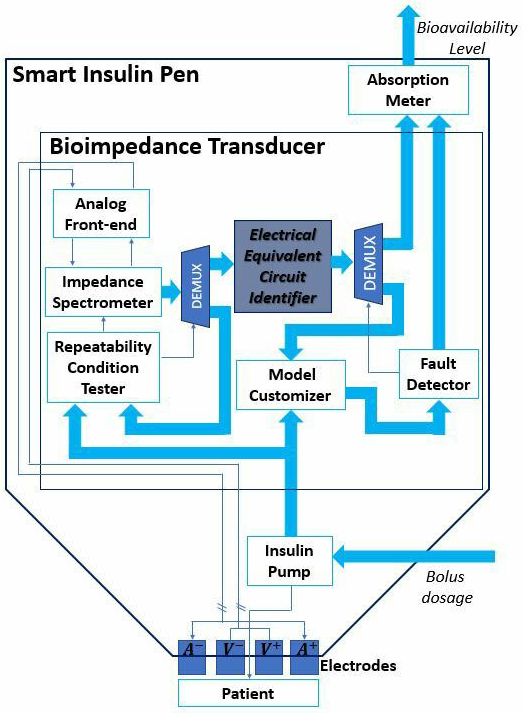


**FIGURE 2. The architecture of the smart insulin pen for non-invasive measurement of artificial insulin absorption.**

In Fig. 2, the architecture of the Bioimpendace Transducer is represented within a Smart Insulin Pen block diagram. The Smart Insulin Pen is equipped with four *Electrodes* positioned around the needle. During bolus administration, four electrodes are applied to the Patient's skin. The *Insulin Pump* injects the insulin bolus articulating it in $n$ different steps. For each injection step, the Insulin Pump transmits the beginning of administration and the dosage of the drug injected to the Bioimpedance Transducer.

The block diagram of the Bioimpedance Transducer is explained below. The Patient is stimulated by an alternating current flowing from the *Impedance Spectrometer* through the $A^-$ and $A^+$ electrodes. The voltage drop is measured by the $V^-$ and $V^+$ electrodes. After the signal conditioning (*Analog Front-End*), the *Repeatability Condition Tester*: (i) sets the Impedance Spectrometer to the single-frequency mode, and (ii) enables the demultiplexer (*DEMUX*) channel dedicated to single-frequency measurements. The Impedance Spectrometer measure the Patient impedance at 10 kHz and transmits the values to the Repeatability Condition Tester. The Repeatability Condition Tester verifies if the 1-$\sigma$ repeatability of six successive acquisitions remains below a threshold empirically determined [32]. Only if acquisitions remain below the threshold, the Repeatability Condition Tester: (i) sets the Impedance Spectrometer to the multi-frequency mode (namely, 100 frequency equispaced in the range [1-100] kHz, logarithmically), and (ii) enables the DEMUX

channel dedicated to multi-frequency measurements [32]. The Impedance Spectrometer gets ten spectra of the Patient and transfers them and the frequency range to the *Electrical Equivalent Circuit Identifier*. Then, the Electrical Equivalent Circuit Identifier: (i) computes the average of the impedance spectra, (ii) finds the best fitting equivalent circuit, and (iii) sends the value of the most sensitive parameter (MSP) to the *Model Customizer*. Subsequently, the Model Customizer builds the function relating: (i) the quantity of drug received from Insulin Pump, and (ii) the MSP value. The *Fault Detector* verifies the parameters of the personalized model founded in the course of the administration. In particular, if the parameters results within the experimentally defined limits [32], the Fault Detector activates the *DEMUX* channel for bioavailability monitoring at the end of the bolus injection. In this way, the *Absorption Meter* computes the amount of drug migrated from the site of injection into the capillary by inverting the personalized model identified.

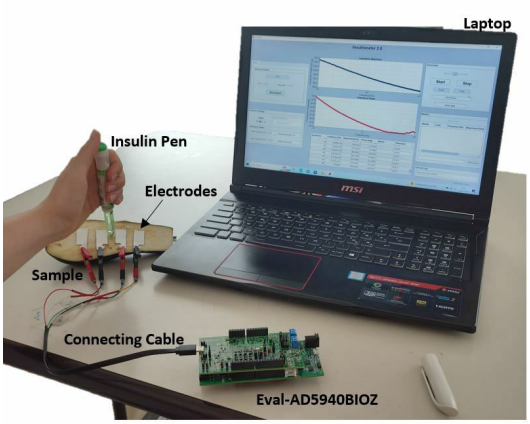


**FIGURE 3.** Experimental set-up: the drug is injected into the sample (eggplant) via the insulin pen, and the impedance is measured by the impedance spectrometer (Eval-AD5940BIOZ) connected to the electrodes applied to the sample. The impedance data are sent via Bluetooth to a laptop where they are plotted by a customised interface.

## IV. IN-VITRO METROLOGICAL CHARACTERIZATION

In this section, the experimental campaign is presented. The aim of the experimental campaign was to investigate the impact of the equivalent circuit approach on the sensitivity of the bioimpedance-based transducer and consequently on the uncertainty of the Smart Insulin Pen. In particular, the experimental setup is described in Section IV-A, and the results are discussed in Section IV-B.

### A. SETUP OF THE EXPERIMENTS

Eggplant pulps were used in the experiments because human skin exhibits similar electrical properties [57]. In particular, the variation of permittivity is negligible in the frequency range of interest (namely, [1-100] kHz) for both eggplants and human skin [58], [59]. The experiments were conducted in a climate-controlled room at 20 °C ± 2 °C and 50 % ± 10 %. The eggplants were subjected to a 2-hours dehydration process at 23 Â°C and then they were sliced in cuboids of length 10 cm, width of 4 cm, and height of 4 cm. The measurements were performed by exploiting the Analog Device EvalAD5940BIOZ in a four-wires configuration (Fig.3) to guarantee a more stable and robust measurement compared to the 2-wires configuration. Indeed, the EVALAD5940BIOZ allows to perform the four-wire measurement by properly setting a low power transimpedance amplifier (TIA) to measure the signal from the sense electrodes [60], [61]. FIAB 500 14 mm × 36 mm electrodes were placed on each eggplant with an inter-electrodic distance of 1 cm. Electrodes were connected to the impedance spectrometer through a 20 cm long cable. The data transmission between the impedance spectrometer and the laptop was guaranteed by the Bluetooth Low Energy 5.0 protocol. The Blutooth protocol is handled by the EM9304 chip situated in the down-board of the Eval-AD5940BIOZ. The laptop was set to battery power mode and simultaneously showed the impedance magnitude and phase trends as the measurement proceeded.

The insulin was administered using a Lilly's Insulin Pen [62] having a 0.4 cm long needle.The infusion needles are disposable and can be assembled on the syringe by means of a plastic holder (namely, *needle hub*) from which the 4 mm needle exits. The deep penetration of the needle was controlled by guaranteeing the contact between the *needle hub* and the surface of the eggplants where the electrodes are positioned. Insulin injections were performed in the centre of the rectangle built on opposite sides (facing each other) of the voltage-sensing electrodes. After the introduction of the needle, the insulin pen was kept perpendicular to the sample to maintain invariant the spacial relationship between electrodes and drug. After each injection performed, the operator stops gripping the syringe and merely holds it perpendicular to the eggplant (namely, keeping the syringe resting on the palm of his hand). In this way, the variation in pressure exerted during the measurements is minimized as it slightly differs from the pressure attributable to the syringe weight. For each eggplant, 14 units of insulin (IU) were injected in 7 consecutive steps of 20 $\mu$l (2 IU). The impedance spectrum of the tissue was measured before the injection (baseline) and after each injection step by fixing the amplitude of the applied signal to 100 mV. For each experimental step ($E_{step}$), ten consecutive impedance spectra were acquired in the range [1-100] kHz divided logarithmically into 100 frequencies. The diffusion process of the drug within the eggplant was excluded as a first approximation due to the limited duration of the experiments (namely, 15 minutes).

As shown in the Bode diagrams of Figs. 4 and 5, the insulin amount exhibits an inverse relationship with impedance magnitude and a direct relationship with impedance phase. The Nyquist diagram of a sample is shown in Fig. 6. The major impact of injection on impedance spectra is visible at low-frequencies when the electrical current flows almost only through extracellular fluid due to the capacitive behaviour of

IEEE Journal of Translational Engineering in Health and Medicine

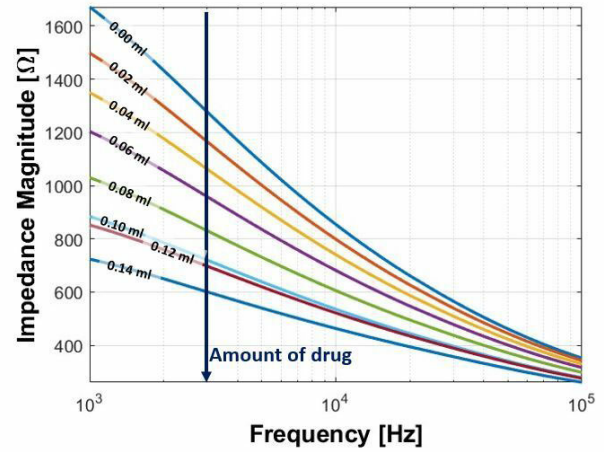


**FIGURE 4.** Impedance magnitude trend of eggplant tissue variation during insulin injections. The amount of drug injected increases in the direction expressed by the blue arrow.

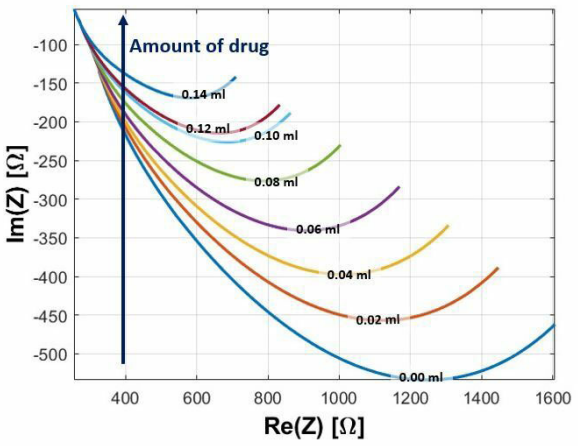


**FIGURE 6.** Impedance spectrum of eggplant tissue variation during insulin injections The amount of drug injected increases in the direction expressed by the blue arrow.

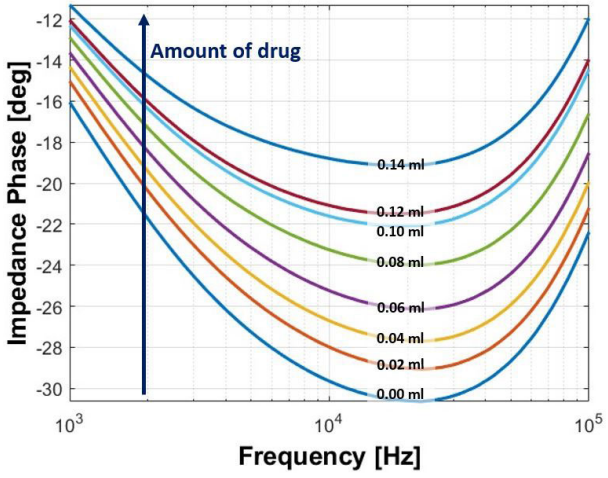


**FIGURE 5.** Impedance phase trend of eggplant tissue variation during insulin injections. The amount of drug injected increases in the direction expressed by the blue arrow.

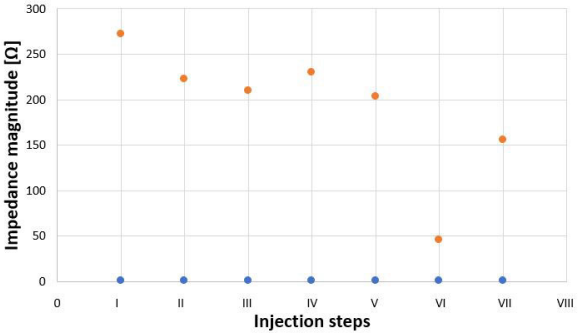


**FIGURE 7.** Comparison between the impact of uncertainty sources and drug injection on impedance magnitude.

the cell membranes. Moreover, the electrical current through intracellular fluid at high-frequencies. In this bandwidth, the impact of insulin injections cannot be appreciated and this supports the hypothesis of a negligible crossing of the cell membrane by insulin.

The effectiveness of the containment of uncertainty sources was illustrated in Fig.7. The orange trend represents the impact of drug introduction on impedance magnitude. In particular, at each step of the injection, the mean of 10 consecutive impedance measurements acquired at 10 kHz was calculated. The impact of drug introduction on impedance magnitude was calculated as the variation between the mean of the current injection step and the mean of the previous one. The blue trend represent the impact of uncertainty sources on impedance magnitude. The impact of uncertainty sources was assessed as the standard deviation over the 10 measurements made after each injection step.

### *B. RESULTS*

For each injection step, the mean of the ten spectra was calculated and used to identify the value of equivalent circuit parameters ($R_e$, $R_i$, T, and p) with Zview software [63]. The Weighting Sum of Squares (type of data weighting = *calc-modulus*) was considered to evaluate the goodness of fit. In this preliminary study of eggplant-based human skin emulation, Zview replaced the Electrical Equivalent Circuit Recognizer block. A comparison between the experimental data and the fitting models before and after the seven injections was reported in Fig. 8.

A preliminary analysis was conducted on $R_e$, $R_i$. CPE-T, CPE-p, and $C_a$ to isolate the equivalent circuit parameter most sensitive to insulin administration. In particular, for each parameter a percentage variation was calculated between the baseline and the value after the seventh injection. The percentage variation was averaged on the ten samples and the standard deviation was computed.Results are reported in Table 1. The high inter-variability between the samples can be related to the different chemical characteristics of the tissue affecting the initial impedance value. As shown in Table 1, CPE-p, CPE-T and $C_a$ alternate between positive

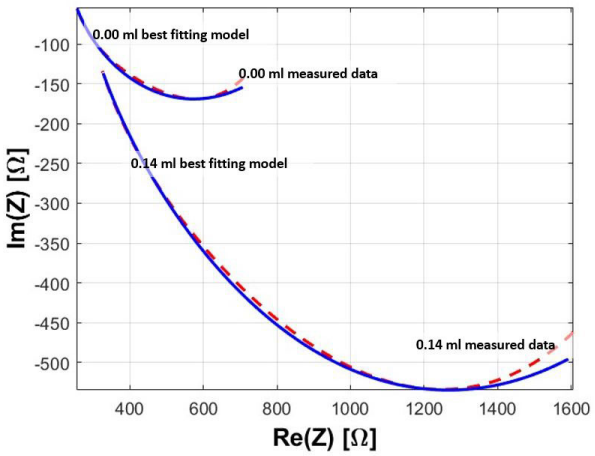


**FIGURE 8.** Comparison between measured (dotted line) and fitted (continuous line) impedance spectra before (0.00 ml) and after the seven injections (0.14 ml).

**TABLE 1.** Percentage variation of equivalent circuit parameters before and after the seventh injections.

| Sample | $R_e$ [%] | $R_i$ [%] | CPE-T [%] | CPE-p [%] | $C_a$ [%] |
|---|---|---|---|---|---|
| **1** | 57.73 | 10.48 | -376.67 | 17.24 | -49.68 |
| **2** | 20.14 | 1.42 | -9.91 | 0.00 | -4.85 |
| **3** | 27.82 | 1.11 | -22.53 | -3.03 | 9.74 |
| **4** | 20.13 | 1.10 | -3.55 | 0.00 | 1.89 |
| **5** | 41.35 | 9.16 | -33.54 | 0.51 | -11.91 |
| **6** | 19.41 | 17.07 | -20.50 | 1.81 | 0.98 |
| **7** | 29.07 | 6.42 | 0.44 | -1.40 | 10.22 |
| **8** | 53.41 | 23.91 | -197.02 | 11.30 | -26.13 |
| **9** | 43.42 | 8.10 | -22.80 | 0.38 | 11.02 |
| **10** | 30.95 | 14.17 | -15.74 | 0.36 | 5.79 |
| Mean | 33.34 | 8.25 | -70.18 | 3.02 | -5.29 |
| Std Dev | 14.80 | 6.96 | 122.20 | 5.83 | 19.42 |

and negative signs of variation and exhibit standard deviation values greater than the mean. $R_e$ resulted more sensitive to insulin injections with respect to $R_i$.

This result is in line with the literature since the electrical component used to model the extracellular fluids resulted the most sensitive to tissue hydration/dehydration and drug accumulation [53], [56], [64]. Then, a relationship between the quantity of insulin administered and the $R_e$ was obtained. In particular, a percentage resistance variation (PRV) was calculated between $R_e$ of each injection step and the baseline. For each sample, a linear relationship between the quantity of insulin administered and the PRV was obtained. Reproducibility, repeatability, sensitivity, nonlinearity, deterministic error, and uncertainty of the bioimpedance-based transducer were calculated for the personalized models.

*Reproducibility:* For each $E_{step}$, the standard deviation of the PRVs was computed. The 1-$\sigma$ reproducibility was obtained as the PRVs' average standard deviation. Then, the percentage with respect to the PRVs' overall mean was calculated. A percentage 1-$\sigma$ reproducibility of 40.98 % was obtained.

**TABLE 2.** Bioimpedance transducer sensitivity and nonlinearity.

| Sample | Sensitivity [ml $^{-1}$] | Nonlinearity [%] |
|---|---|---|
| **1** | 391.14 | 17.50 |
| **2** | 126.04 | 6.45 |
| **3** | 125.43 | 6.29 |
| **4** | 133.35 | 6.45 |
| **5** | 314.13 | 12.32 |
| **6** | 161.92 | 2.39 |
| **7** | 187.26 | 7.11 |
| **8** | 366.32 | 9.77 |
| **9** | 269.44 | 9.31 |
| **10** | 184.00 | 6.66 |

*Repeatability:* For each $E_{step}$, ten impedance spectra were measured, the related $R_e$ value were calculated and inserted into a vector (one vector for baseline ($v_1$) and seven for the seven consecutive administrations ($v_{i1}$,$v_{i2}$, …, $v_{i7}$)). For each vector, the mean and the standard deviation were calculated and stored in further vectors (one vector for the average ($v_{mean}$) and seven vectors for the standard deviations ($v_{std}$)). Then, the percentage 1-$\sigma$ repeatability was computed as percentage ratio between the average of $v_{std}$ and the average of $v_{mean}$. A mean percentage 1-$\sigma$ repeatability of 0.78 % was obtained.

*Sensitivity:* The sensitivity was computed as the slope of personalized models identified. Table 2 illustrates the results obtained for each experimental sample while Fig.9 reports a comparison between the mean and a specific sample PRV trend at increasing the quantity of insulin administered. In particular, Fig. 9.A represents the mean trend and the standard deviation calculated among the ten samples; the huge error bars underline the wide 1-$\sigma$ reproducibility if a general model is implied. Fig. 9.B represents the personalized trend of a sample. In this case the error bar are very small as a consequence of the model customization process.

Even if the personalized models are different, a minimum sensitivity of 125.43 $ml^{-1}$ compared to mean value of 225.91 $ml^{-1}$ emerged from the experimental campaign. The main factors impacting on the sensitivity can be related to the chemical characteristic of the drug (ionic charge, viscosity, ecc.) and the characteristic of the experimental setup (proximity of the injected drug to the point of maximum current density).

*Nonlinearity:* The following equation was used to compute the nonlinearity:

$$\sqrt{\frac{\sum_{i=1}^{k}(y_i - \widehat{y}_i)^2}{k-2}} \tag{6}$$

where:

- k represents the seventh injections;
- y the PRV obtained from experimental data;
- $\widehat{y}$ the PRV computed with the equation of personalized model.

Subsequently, the percentage nonlinearity was computed as the percentage ratio between the nonlinearity value and

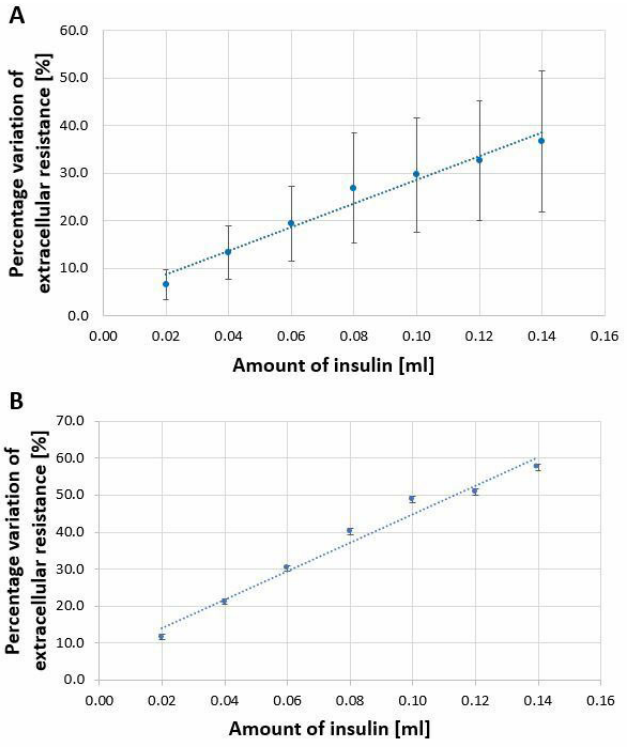


**FIGURE 9.** Comparison between the mean (A) and specific sample (B) PRV trend at increasing the quantity of insulin administered.

range of percentage resistance variation. The results are reported in Table 2.

*Deterministic Error:* For each personalized model, the root-mean-square error (RMSE) was computed and then averaged between models (MRMSE). A mean MRMSE of 2.78 % was obtained.

*Uncertainty:* Two major sources of uncertainty were considered: (i) measurand, and (ii) instrument. The measurand uncertainty ($u_m$) was computed as the percentage 1-$\sigma$ repeatability with respect to the square root of the repeated measurements (namely 10). The instrument uncertainty ($u_i$) was computed as the percentage 1-$\sigma$ repeatability at 10000 Hz resulted from calibration measurements with respect to the square root of the number of repeated measurements (namely 10). The uncertainty was computed as positive square root of the combined variance $(u_m)^2$ and $(u_i)^2$. An uncertainty of 0.25 % was obtained.

In Table 3, the proposed BIS-method is compared to the BIA-method validated in [32]. Except for the repeatability and uncertainty, all the metrological parameters of the bioimpedance transducer improved with the new method based on BIS measurement and equivalent circuit approach. In particular, the sensitivity increased by 223 % for sensitivity, and the deterministic error decreased by 45 %. As concern the repeatability and uncertainty, the worsening is due to the new uncertainty source, namely the electrical equivalent circuit procedure.

**TABLE 3.** Comparison between the metrological parameters of the bioimpedance transducer in case of (i) BIS-measurements, and (ii) BIA-measurements.

| Parameter | BIA-based method [32] | BIS-based method |
|---|---|---|
| Reproducibility | 71.00 % | 40.98 % |
| Repeatability | 0.45 % | 0.78 % |
| Sensitivity | 69.98 $ml^{-1}$ | 225.90 $ml^{-1}$ |
| nonlinearity | 9.03 % | 8.43 % |
| Determinist error | 5.00 % | 2.78 % |
| Uncertainty | 0.14 % | 0.25 % |

### C. SMART INSULIN PEN UNCERTAINTY

The Absorption Meter: 1) receives the personalised model from the Fault Detector, 2) inverts it, and 3) associates the estimated residual drug quantities with $R_e$ values received from the Electrical Equivalent Circuit Identifier. The uncertainty of the personalized model ($u_{mp}$) propagates on the residual drug measurement. The uncertainty on the residual drug measurement ($u_{drug}$) is calculated from $u_{mp}$ by taking into account the inversion of the personalized model, namely by dividing $u_{mp}$ by the sensitivity of the model. Thus, the wide gain in sensitivity due to the electrical equivalent circuit results in a significant reduction of $u_{drug}$. In the case of the emulation performed on eggplants, the improvement in sensitivity was 223 %. Considering the same proportions in in-vivo applications, a decrement of $u_{drug}$ from 4.2 $\mu$l ([32]) to 1.3 $\mu$l would be expected and the variation of drug could be detected even a short time after injections.

### D. DISCUSSION

The electrical equivalent circuit approach achieved a significant improvement of a bioimpedance transducer compared to previous experimental work [32]. Despite having validated the method only on eggplants, the compatibility between the electrical response of eggplant and humans to insulin injection has been proven in other studies [32], [65]. Indeed, eggplants introduced some limitations to the analysis. For example, vegetables are not subject to mechanical noise sources (e.g., breathing) or metabolic processes. Moreover, the electrical properties do not entirely mimic the metabolic and enzymatic processes that can influence insulin dynamics in human tissue. However, even taking into account these limitations, the comparability between eggplants and human tissue is only assessed with reference to the injection phase. In this phase, a quasi-static approximation of human tissue metabolic behavior can be assumed. Indeed, the measuring time is much lower than the average time needed to absorb 6 units of insulin [66]. Although the proven compatibility between the electrical response of eggplant and human, the method presented in this paper has not yet been validated on humans. In this case, the adaptability to the different physiological conditions of patients will be crucial for achieving clinical impact. The equivalent circuit approach is suitable for identifying personalized models that can handle the variability of individual responses to insulin. Indeed, after identifying a suitable model that effectively describes the

electrical behavior of human tissue, spectrum measurements can be used to identify the electrical parameters specific to the particular patient.Nevertheless, an extensive experimental campaign will be necessary to validate the capability of the proposed system to identify specific characteristics of patients in terms of corresponding electrical parameters.

## V. CONCLUSION

The metrological characteristics of a bioimpedance-based transducer for quantifying insulin in eggplants were improved using the equivalent circuit approach. The emulation of human tissue by eggplants was assumed because the measuring time was kept much lower than the typical insulin absorption time (quasi-static approximation). The Modified Hayden's model was adopted as a reference circuit. The electrical component used to model the extracellular fluids was identified as the most sensitive parameter to insulin injections. An improvement of 223 % in sensitivity due to the electrical equivalent circuit results in a significant uncertainty reduction. The transducer is designed to be integrated into a Smart Insulin Pen for real-time measurements of insulin bioavailability. Considering the same improvement of sensitivity in in-vivo applications, the uncertainty of the Smart Insulin Pen is decreased from 4.2 $\mu$l to 1.3 $\mu$l. Experimental campaigns on diabetic patients are underway to validate the method on humans.

## ACKNOWLEDGMENT

The IEEE Instrumentation and Measurement Graduate Fellowship Award 2022 supported this research.

## REFERENCES

[1] I. D. Federation. *International Diabetes Federation*. Accessed: Oct. 10, 2023. [Online]. Available: https://idf.org/about-diabetes/type-1-diabetes/

[2] J. A. Bluestone, K. Herold, and G. Eisenbarth, "Genetics, pathogenesis and clinical interventions in type 1 diabetes," *Nature*, vol. 464, no. 7293, pp. 1293–1300, Apr. 2010.

[3] J. A. Todd, "Etiology of type 1 diabetes," *Immunity*, vol. 32, no. 4, pp. 457–467, Apr. 2010.

[4] T. Karacolak, A. Z. Hood, and E. Topsakal, "Design of a dual-band implantable antenna and development of skin mimicking gels for continuous glucose monitoring," *IEEE Trans. Microw. Theory Techn.*, vol. 56, no. 4, pp. 1001–1008, Apr. 2008.

[5] I. B. Hirsch, "Realistic expectations and practical use of continuous glucose monitoring for the endocrinologist," *J. Clin. Endocrinol. Metabolism*, vol. 94, no. 7, pp. 2232–2238, Jul. 2009.

[6] K. K. Adhikari and N.-Y. Kim, "Ultrahigh-sensitivity mediator-free biosensor based on a microfabricated microwave resonator for the detection of micromolar glucose concentrations," *IEEE Trans. Microw. Theory Techn.*, vol. 64, no. 1, pp. 319–327, Jan. 2016.

[7] M. Baghelani, Z. Abbasi, M. Daneshmand, and P. E. Light, "Non-invasive continuous-time glucose monitoring system using a chipless printable sensor based on split ring microwave resonators," *Sci. Rep.*, vol. 10, no. 1, pp. 1–15, Jul. 2020.

[8] N.-Y. Kim, K. K. Adhikari, R. Dhakal, Z. Chuluunbaatar, C. Wang, and E.-S. Kim, "Rapid, sensitive and reusable detection of glucose by a robust radiofrequency integrated passive device biosensor chip," *Sci. Rep.*, vol. 5, no. 1, pp. 1–9, Jan. 2015.

[9] V. Katseli, A. Economou, and C. Kokkinos, "Smartphone-addressable 3D-printed electrochemical ring for nonenzymatic self-monitoring of glucose in human sweat," *Anal. Chem.*, vol. 93, no. 7, pp. 3331–3336, Feb. 2021.

[10] J. Yadav, A. Rani, V. Singh, and B. M. Murari, "Prospects and limitations of non-invasive blood glucose monitoring using near-infrared spectroscopy," *Biomed. Signal Process. Control*, vol. 18, pp. 214–227, Apr. 2015.

[11] N. Spegazzini et al., "Spectroscopic approach for dynamic bioanalyte tracking with minimal concentration information," *Sci. Rep.*, vol. 4, no. 1, pp. 1–7, Nov. 2014.

[12] W. Villena Gonzales, A. Mobashsher, and A. Abbosh, "The progress of glucose monitoring—A review of invasive to minimally and non-invasive techniques, devices and sensors," *Sensors*, vol. 19, no. 4, p. 800, Feb. 2019.

[13] C. Cobelli, E. Renard, and B. Kovatchev, "Artificial pancreas: Past, present, future," *Diabetes*, vol. 60, no. 11, pp. 2672–2682, Nov. 2011.

[14] R. J. Young, W. J. Hannan, B. M. Frier, J. M. Steel, and L. J. P. Duncan, "Diabetic lipohypertrophy delays insulin absorption," *Diabetes Care*, vol. 7, no. 5, pp. 479–480, Sep. 1984.

[15] T. Heise, E. Zijlstra, L. Nosek, S. Heckermann, L. Plum-Mörschel, and T. Forst, "Euglycaemic glucose clamp: What it can and cannot do, and how to do it," *Diabetes, Obesity Metabolism*, vol. 18, no. 10, pp. 962–972, Oct. 2016.

[16] R. A. DeFronzo, J. D. Tobin, and R. Andres, "Glucose clamp technique: A method for quantifying insulin secretion and resistance," *Amer. J. Physiol.-Endocrinol. Metabolism*, vol. 237, no. 3, p. 214, Sep. 1979.

[17] L. Heinemann and J. H. Anderson, "Measurement of insulin absorption and insulin action," *Diabetes Technol. Therapeutics*, vol. 6, no. 5, pp. 698–718, Oct. 2004.

[18] P. Hildebrandt and K. Birch, "Basal rate subcutaneous insulin infusion: Absorption kinetics and relation to local blood flow," *Diabetic Med.*, vol. 5, no. 5, pp. 434–440, Jul. 1988.

[19] E. Mosekilde, K. S. Jensen, C. Binder, S. Pramming, and B. Thorsteinsson, "Modeling absorption kinetics of subcutaneous injected soluble insulin," *J. Pharmacokinetics Biopharmaceutics*, vol. 17, no. 1, pp. 67–87, Feb. 1989.

[20] M. Schiavon, C. Dalla Man, and C. Cobelli, "Modeling subcutaneous absorption of fast-acting insulin in type 1 diabetes," *IEEE Trans. Biomed. Eng.*, vol. 65, no. 9, pp. 2079–2086, Sep. 2018.

[21] L. Ayalew et al., "C-terminal lysine processing of IgG in human suction blister fluid: Implications for subcutaneous administration," *Mol. Pharmaceutics*, vol. 19, no. 11, pp. 4043–4054, Nov. 2022.

[22] S. Eirefelt et al., "Evaluating dermal pharmacokinetics and pharmacodynamic effect of soft topical PDE4 inhibitors: Open flow microperfusion and skin biopsies," *Pharmaceutical Res.*, vol. 37, no. 12, pp. 1–12, Dec. 2020.

[23] S. F. Cordery et al., "Topical bioavailability of diclofenac from locally-acting, dermatological formulations," *Int. J. Pharmaceutics*, vol. 529, nos. 1–2, pp. 55–64, Aug. 2017.

[24] B. A. Kuzma, S. Senemar, T. Ramezanli, P. Ghosh, S. G. Raney, and G. Stagni, "Evaluation of local bioavailability of metronidazole from topical formulations using dermal microdialysis: Preliminary study in a Yucatan mini-pig model," *Eur. J. Pharmaceutical Sci.*, vol. 159, Apr. 2021, Art. no. 105741.

[25] S. Y. Chaw, T. T. L. Wong, S. Venkatraman, and A.-M. Chacko, "Spatio-temporal in vivo imaging of ocular drug delivery systems using fiberoptic confocal laser microendoscopy," *J. Visualized Exp.*, vol. 175, Sep. 2021, Art. no. e62685.

[26] M. N. Afsar, A. Moonshiram, and Y. Wang, "Assessment of random and systematic errors in millimeter-wave dielectric measurement using open resonator and Fourier transform spectroscopy systems," *IEEE Trans. Instrum. Meas.*, vol. 53, no. 4, pp. 899–906, Aug. 2004.

[27] U. A. Khan, N. Nguyen, and M. N. Afsar, "Millimeter-and submillimeter-wave dielectric measurements of household powders using Fourier transform spectroscopy," *IEEE Trans. Instrum. Meas.*, vol. 57, no. 2, pp. 286–293, Feb. 2008.

[28] D. Das, F. A. Kamil, S. Agrawal, K. Biswas, and S. Das, "Fragmental frequency analysis method to estimate electrical cell parameters from bioimpedance study," *IEEE Trans. Instrum. Meas.*, vol. 63, no. 8, pp. 1991–2000, Aug. 2014.

[29] D. Chowdhury and M. Chattopadhyay, "Study and classification of cell bio-impedance signature for identification of malignancy using artificial neural network," *IEEE Trans. Instrum. Meas.*, vol. 70, pp. 1–8, 2021.

[30] R. Baghbani, M. B. Shadmehr, M. Ashoorirad, S. F. Molaeezadeh, and M. H. Moradi, "Bioimpedance spectroscopy measurement and classification of lung tissue to identify pulmonary nodules," *IEEE Trans. Instrum. Meas.*, vol. 70, pp. 1–7, 2021.

[31] G. Annuzzi et al., "Measuring insulin absorption by impedance spectroscopy. A feasibility study," in *Proc. IEEE Int. Symp. Med. Meas. Appl. (MeMeA)*, Jun. 2022, pp. 1–5.

[32] P. Arpaia, F. Mancino, and N. Moccaldi, "A reproducible bioimpedance transducer for insulin noninvasive measurement," *IEEE Trans. Instrum. Meas.*, vol. 72, pp. 1–11, 2023.

[33] P. Arpaia, D. Cuneo, F. Mancino, and N. Moccaldi, "A bioimpedance-based transducer for insulin bioavailability assessment after subcutaneous administration," in *Proc. IEEE Int. Instrum. Meas. Technol. Conf. (IMTC)*, May 2022, pp. 1–5.

[34] R. Hilgenfeld, G. Seipke, H. Berchtold, and D. R. Owens, "The evolution of insulin glargine and its continuing contribution to diabetes care," *Drugs*, vol. 74, no. 8, pp. 911–927, Jun. 2014.

[35] A. C. Buchholz, C. Bartok, and D. A. Schoeller, "The validity of bioelectrical impedance models in clinical populations," *Nutrition Clin. Pract.*, vol. 19, no. 5, pp. 433–446, Oct. 2004.

[36] M. Y. Jaffrin and H. Morel, "Body fluid volumes measurements by impedance: A review of bioimpedance spectroscopy (BIS) and bioimpedance analysis (BIA) methods," *Med. Eng. Phys.*, vol. 30, no. 10, pp. 1257–1269, Dec. 2008.

[37] J.-J. Cabrera-López and J. Velasco-Medina, "Structured approach and impedance spectroscopy microsystem for fractional-order electrical characterization of vegetable tissues," *IEEE Trans. Instrum. Meas.*, vol. 69, no. 2, pp. 469–478, Feb. 2020.

[38] C. Tan, S. Liu, J. Jia, and F. Dong, "A wideband electrical impedance tomography system based on sensitive bioimpedance spectrum bandwidth," *IEEE Trans. Instrum. Meas.*, vol. 69, no. 1, pp. 144–154, Jan. 2020.

[39] P. Arpaia, U. Cesaro, and N. Moccaldi, "Noninvasive measurement of transdermal drug delivery by impedance spectroscopy," *Sci. Rep.*, vol. 7, no. 1, pp. 1–10, Mar. 2017.

[40] R. I. Hayden, C. A. Moyse, F. W. Calder, D. P. Crawford, and D. S. Fensom, "Electrical impedance studies on potato and alfalfa tissue," *J. Experim. Botany*, vol. 20, no. 2, pp. 177–200, 1969.

[41] M. I. N. Zhang, T. Repo, J. H. M. Willison, and S. Sutinen, "Electrical impedance analysis in plant tissues: On the biological meaning of cole–cole $\alpha$ in scots pine needles," *Eur. Biophys. J.*, vol. 24, no. 2, pp. 99–106, Oct. 1995.

[42] H. Lodish, A. Berk, S. L. Zipursky, P. Matsudaira, D. Baltimore, and J. Darnell, "Molecular cell biology 4th edition," *Nat. Center Biotechnol. Inf., Bookshelf*, vol. 9, pp. 199–260, 2000.

[43] T. K. Bera, N. Jampana, and G. Lubineau, "A LabVIEW-based electrical bioimpedance spectroscopic data interpreter (LEBISDI) for biological tissue impedance analysis and equivalent circuit modelling," *J. Electr. Bioimpedance*, vol. 7, no. 1, pp. 35–54, Aug. 2019.

[44] N. Chaffey et al., *Molecular Biology of the Cell*. 4th ed., Oxford Academic, 2003.

[45] L. M. Roa et al., "Applications of bioimpedance to end stage renal disease (ESRD)," in *Modelling and Control of Dialysis Systems: Volume 1: Modeling Techniques of Hemodialysis Systems*. Cham, Switzerland: Springer, 2013, pp. 689–769.

[46] J. Castizo-Olier, A. Irurtia, M. Jemni, M. Carrasco-Marginet, R. Fernández-García, and F. A. Rodríguez, "Bioelectrical impedance vector analysis (BIVA) in sport and exercise: Systematic review and future perspectives," *PLoS ONE*, vol. 13, no. 6, Jun. 2018, Art. no. e0197957.

[47] R. E. Hayden, L. Dionne, and D. S. Fensom, "Electrical impedance studies of stem tissue of solanum clones during cooling," *Can. J. Botany*, vol. 50, no. 7, pp. 1547–1554, Jul. 1972.

[48] T. Watanabe, N. Nakamura, Y. Ando, T. Kaneta, H. Kitazawa, and T. Shiina, "Application and simplification of cell-based equivalent circuit model analysis of electrical impedance for assessment of drop shock bruising in Japanese pear tissues," *Food Bioprocess Technol.*, vol. 11, no. 11, pp. 2125–2129, Nov. 2018.

[49] Y. Ando, K. Mizutani, and N. Wakatsuki, "Electrical impedance analysis of potato tissues during drying," *J. Food Eng.*, vol. 121, pp. 24–31, Jan. 2014.

[50] Y. Ando, Y. Maeda, K. Mizutani, N. Wakatsuki, S. Hagiwara, and H. Nabetani, "Impact of blanching and freeze-thaw pretreatment on drying rate of carrot roots in relation to changes in cell membrane function and cell wall structure," *LWT-Food Sci. Technol.*, vol. 71, pp. 40–46, Sep. 2016.

[51] C. H. Hsu and F. Mansfeld, "Technical note: Concerning the conversion of the constant phase element parameter Y0into a capacitance," *Corrosion*, vol. 57, no. 9, pp. 747–748, Sep. 2001.

[52] S. Mancuso and E. Rinaldelli, "Response of young mycorrhizal and non-mycorrhizal plants of olive tree (*Olea europaea* L.) to saline conditions. II. Dynamics of electrical impedance parameters of shoots and leaves," *Adv. Horticultural Sci.*, vol. 10, pp. 135–145, Jan. 1996.

[53] A. Chowdhury, T. Kanti Bera, D. Ghoshal, and B. Chakraborty, "Electrical impedance variations in banana ripening: An analytical study with electrical impedance spectroscopy," *J. Food Process Eng.*, vol. 40, no. 2, Apr. 2017, Art. no. e12387.

[54] L. Wu, Y. Ogawa, and A. Tagawa, "Electrical impedance spectroscopy analysis of eggplant pulp and effects of drying and freezing–thawing treatments on its impedance characteristics," *J. Food Eng.*, vol. 87, no. 2, pp. 274–280, Jul. 2008.

[55] T. Imaizumi, F. Tanaka, D. Hamanaka, Y. Sato, and T. Uchino, "Effects of hot water treatment on electrical properties, cell membrane structure and texture of potato tubers," *J. Food Eng.*, vol. 162, pp. 56–62, Oct. 2015.

[56] M. Islam, K. A. Wahid, A. V. Dinh, and P. Bhowmik, "Model of dehydration and assessment of moisture content on onion using EIS," *J. Food Sci. Technol.*, vol. 56, no. 6, pp. 2814–2824, Jun. 2019.

[57] B. Rigaud, J.-P. Morucci, and N. Chauveau, "Bioelectrical impedance techniques in medicine—Part I: Bioimpedance measurement second section: Impedance spectrometry," *Crit. Rev. Biomed. Eng.*, vol. 24, nos. 4–6, pp. 257–351, 1996.

[58] P. Hasgall et al., "It'is database for thermal and electromagnetic parameters of biological tissues, version 4.1," Found. Res. Inf. Technol. Soc. (IT'IS), Zürich, Switzerland, 2018.

[59] D. El Khaled, N. N. Castellano, J. A. Gazquez, R. M. G. Salvador, and F. Manzano-Agugliaro, "Cleaner quality control system using bioimpedance methods: A review for fruits and vegetables," *J. Cleaner Prod.*, vol. 140, pp. 1749–1762, Jan. 2017.

[60] *Analoge*. Accessed: Apr. 14, 2024. [Online]. Available: https://www.analog.com/media/en/technical-documentation/data-sheets/ad5940-5941.pdf

[61] *Analoge*. Accessed: Apr. 14, 2024. [Online]. Available: https://www.analog.com/en/resources/app-notes/an-1557.html

[62] *Lilly*. Accessed: Apr. 14, 2024. [Online]. Available: https://www.lilly.it/

[63] *Zview*. Accessed: Oct. 10, 2023. [Online]. Available: https://www.scribner.com/software/68-general-electrochemistr376-zview-for-windows/

[64] K. Song, U. Ha, J. Lee, K. Bong, and H.-J. Yoo, "An 87-mA·min iontophoresis controller IC with dual-mode impedance sensor for patch-type transdermal drug delivery system," *IEEE J. Solid-State Circuits*, vol. 49, no. 1, pp. 167–178, Jan. 2014.

[65] P. Arpaia, F. Galdieri, F. Mancino, and N. Moccaldi, "Enhancing inter-subject reproducibility in insulin bioavailability measurements through real-time calibration," *Measurement*, vol. 231, May 2024, Art. no. 114603.

[66] C. Binder, T. Lauritzen, O. Faber, and S. Pramming, "Insulin pharmacokinetics," *Diabetes Care*, vol. 7, no. 2, pp. 188–199, 1984.

Open Access funding provided by 'Università degli Studi di Napoli ''Federico II''' within the CRUI-CARE Agreement